J Biomol NMR (2008) 40:157–163
DOI 10.1007/s10858-008-9224-8

COMMUNICATION

GFT projection NMR based resonance assignment of membrane proteins: application to subunit c of *E. coli* F_1F_0 ATP synthase in LPPG micelles

Qi Zhang · Hanudatta S. Atreya · Douglas E. Kamen · Mark E. Girvin · Thomas Szyperski

Received: 29 November 2007 / Accepted: 23 January 2008 / Published online: 14 February 2008

Abstract G-matrix FT projection NMR spectroscopy was employed for resonance assignment of the 79-residue subunit c of the *Escherichia coli* F_1F_0 ATP synthase embedded in micelles formed by lyso palmitoyl phosphatidyl glycerol (LPPG). Five GFT NMR experiments, that is, (3,2)D HNNCO, L-(4,3)D HNN$C^{\alpha\beta}C^{\alpha}$, L-(4,3)D HNN(CO)$C^{\alpha\beta}C^{\alpha}$, (4,2)D HACA(CO)NHN and (4,3)D HCCH, were acquired along with simultaneous 3D ^{15}N, $^{13}C^{aliphatic}$, $^{13}C^{aromatic}$-resolved [^{1}H,^{1}H]-NOESY with a total measurement time of ~43 h. Data analysis resulted in sequence specific assignments for all routinely measured backbone and $^{13}C^{\beta}$ shifts, and for 97% of the side chain shifts. Moreover, the use of two G^{2}FT NMR experiments, that is, (5,3)D HN{N,CO}{$C^{\alpha\beta}C^{\alpha}$} and (5,3)D {$C^{\alpha\beta}C^{\alpha}$}{CON}HN, was explored to break the very high chemical shift degeneracy typically encountered for membrane proteins. It is shown that the 4D and 5D spectral information obtained rapidly from GFT and G^{2}FT NMR experiments enables one to efficiently obtain (nearly) complete resonance assignments of membrane proteins.

Keywords Membrane protein · GFT NMR · Projection NMR · Resonance assignment · Subunit c · F_1F_0 ATP synthase · LPPG

Abbreviations

GFT	G-matrix Fourier transformation
LPPG	1-Palmitoyl-2-hydroxy-sn-glycero-3-[phospho-RAC-(1-glycerol)]
RAC	Racemic

Even though 20–30% of a typical proteome are membrane proteins, which are pivotal for living cellular systems and constitute 60–70% of current drug targets (Lundstrom 2007), less than 0.5% of all atomic resolution structures in the PDB are from membrane proteins (Granseth et al. 2007). This reflects the tremendous difficulties encountered for structure determination of membrane proteins, in particular when envisaging structural genomics of membrane proteins. To resolve key bottlenecks, the National Institutes of Health in the United States has funded 'specialized centers' for methodology development, such as the New York Consortium of Membrane Protein Structure (NYCOMPS) (http://www.nycomps.org).

For NMR-based membrane protein structure determination, the preparation of $^{13}C/^{15}N$-labeled protein samples is required along with suitable protocols for reconstituting the purified membrane protein into a membrane mimic (e.g., Krueger-Koplin et al. 2004). Subsequently, either solution or solid-state NMR can be used to obtain a high-quality NMR structure (e.g., Sorgen et al. 2002; Tamm et al. 2003; Fernandez et al. 2004; Gao and Cross 2005). For both approaches, however, the severe chemical shift

Qi Zhang, Hanudatta S. Atreya, Douglas E. Kamen, Mark E. Girvin and Thomas Szyperski—New York Consortium on Membrane Protein Structure.

Q. Zhang · H. S. Atreya · T. Szyperski (✉)
Department of Chemistry, State University of New York at Buffalo, Buffalo, NY 14260, USA
e-mail: szypersk@chem.buffalo.edu

Present Address:
H. S. Atreya
NMR Research Centre, Indian Institute of Science, Bangalore 560012, India

D. E. Kamen · M. E. Girvin
Biochemistry Department, Albert Einstein College of Medicine, New York, NY 10461, USA

degeneracy encountered for membrane proteins impedes data analysis. The degeneracy arises from the rather narrow amino acid composition of membrane proteins (Fig. 1; Tourasse and Li 2000) and the fact that α-helices show per se more limited shift dispersion than extended β-strands (Cavanagh et al. 2007).

Hence, it was proposed to employ GFT projection NMR spectroscopy (Kim and Szyperski 2003; Atreya and Szyperski 2004, 2005; Eletsky et al. 2005; Shen et al. 2005; Szyperski and Atreya 2006) for rapidly obtaining the precise highest-dimensional NMR spectral information for breaking the very high shift degeneracy (Atreya et al. 2005). The G-matrix transformation, which is required to phase-sensitively detect linear combinations of chemical shifts for an arbitrary number of spins in a pure absorption mode, allows one to acquire five or higher-dimensional spectral information (Kim and Szyperski 2003). Other valuable approaches requiring G-matrix transformations include (i) projection-reconstruction NMR (Kupce and Freeman 2004), taking advantage of the option to scale the jointly sampled shifts (e.g. Kim and Szyperski 2003; Atreya and Szyperski 2005), (ii) 'Automated projection NMR' (Hiller et al. 2005), and (iii) Hi-Fi NMR (Eghbalnia et al. 2005).

The two transmembrane-helix subunit c of the F_0 portion of the ATP synthase is involved in both proton translocation across the membrane and in coupling this proton flux to ATP synthesis by the F_1 complex. Hence there has been great interest in its structure and in any possible protonation-linked conformational changes. Resonance assignments, secondary structures and solution structures have been reported for the c subunits of *E. coli* (Norwood et al 1992; Girvin et al 1998; Rastogi and Girvin 1999a, b; Dmitriev et al. 2002; Dmitriev and Fillingame 2001), *P. modestum* (Matthey et al. 2002), *B. firmus* OF4 (Rivera-Torres et al. 2004), and *Bacillus* PS3 (Nakano et al. 2006) in chloroform–methanol–water or chloroform–methanol solvent mixtures, while the only study in detergent micelles published thus far has been for the sodium-transporting c subunit from *P. modestum* reconstituted in SDS micelles (Matthey et al. 1999). In this communication, we describe the utility of GFT NMR for obtaining essentially complete resonance assignments for multi-span helical membrane proteins, using the subunit c (D61 → N) of the *Escherichia coli* F_1F_0 ATP synthase reconstituted in LPPG micelles (Krueger-Koplin et al. 2004). The D61 → N mutation mimics a protonated side chain at neutral pH.

The NMR sample was prepared by dissolving (i) 2.5 mg $^{13}C,^{15}N$-labeled protein in 1:1 chloroform/methanol and (ii) 15 mg LPPG (Avanti Polar Lipids, Alabaster, USA) in chloroform, followed by drying the mixture of the two solution under an argon stream (Krueger-Koplin et al. 2004). The resultant film was dissolved in 300 µl of 90% H_2O/10% ^2H_2O (50 mM potassium phosphate; pH = 7.0), yielding an ~0.9 mM protein solution. The corresponding 2D [$^{15}N,^1H$] HSQC spectrum (Fig. 2) shows that a homogenous sample was obtained. The rotational correlation time of the subunit c-micelle system was shown previously to correspond to a globular protein of ca.

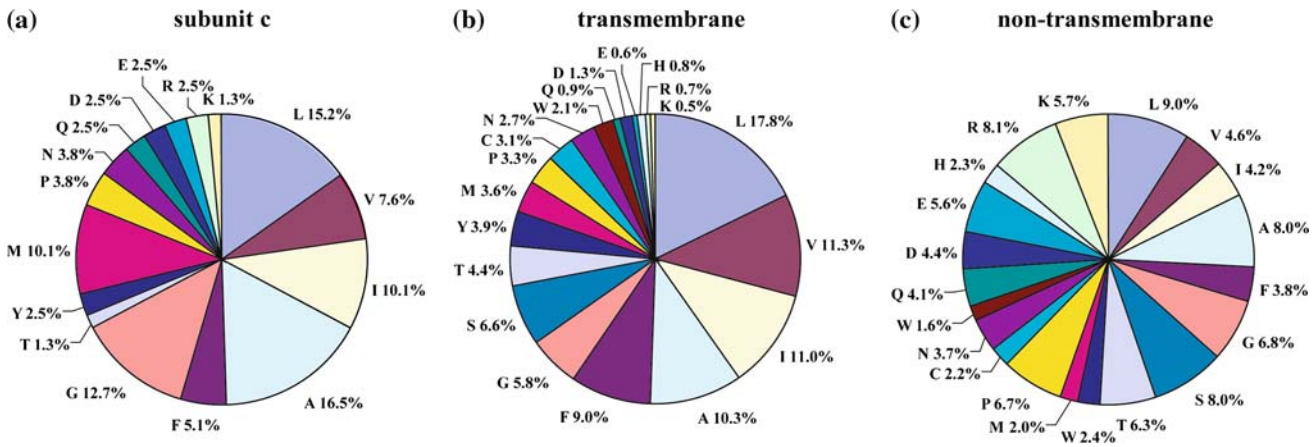

Fig. 1 Amino acid composition in the one-letter code of (**a**) subunit c of *E. coli* ATP synthase, (**b**) trans-membrane helices (Tourasse and Li 2000), and (**c**) non-membrane proteins (Tourasse and Li 2000). The uniformity of the amino acid compositions can be quantitatively assessed by calculation the Shannon entropy of information theory (Shannon 1948), S, of the compositions according to $S = -\sum_i p_i \log p_i$, where p_i represents the fraction of amino acid i. This yields S(subunit c) = 1.08, S(transmembrane) = 1.13 and S(non-transmembrane) = 1.25. Considering that S must be between 0 (a single $p_i = 1$) and 1.301 (all $p_i = 0.05$), these values reflect the rather uniform amino acid composition of transmembrane helices, which contributes to the very high chemical shift degeneracy (see text). Furthermore, the values show that the composition of subunit c is even more uniform that the average composition of helical transmembrane proteins, and it might be that entropy is a valuable quantitative measure to estimate shift degeneracy emerging from uniformity of amino acid composition

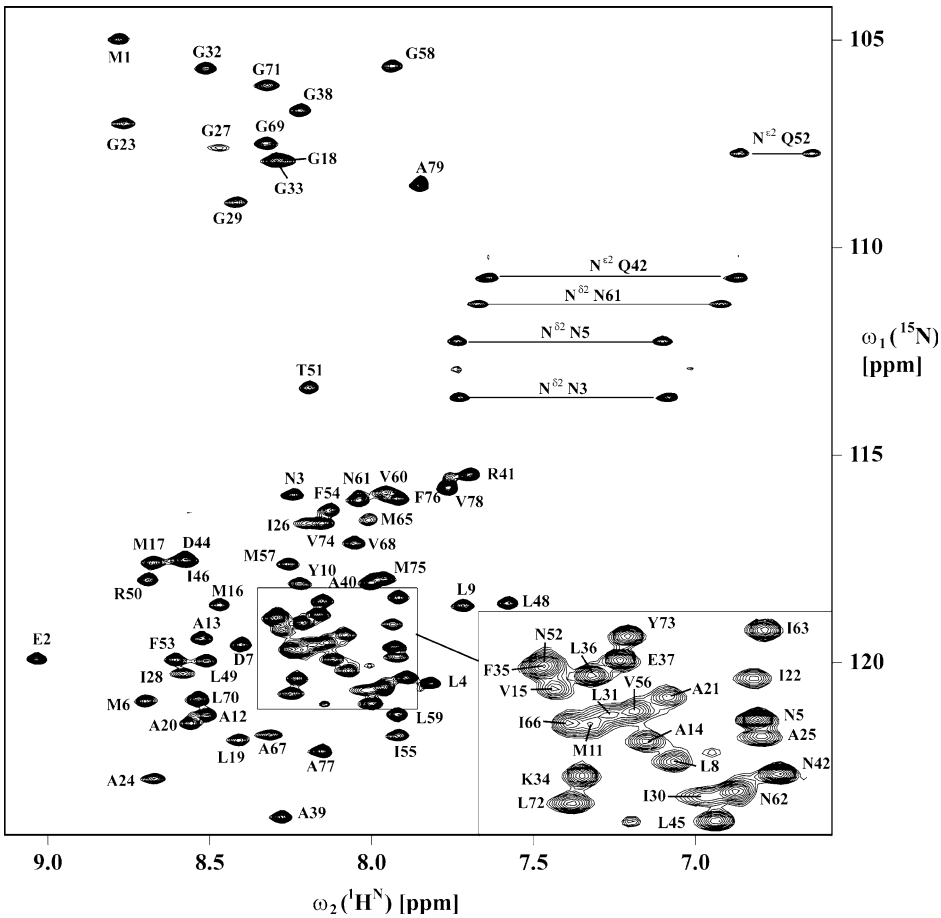

Fig. 2 2D [^{15}N,^{1}H] HSQC spectrum recorded at 45°C for subunit c of *E. coli* F_1F_0 ATP synthase reconstituted in LPPG micelles. Resonance assignments are given in the one-letter amino acid code and residue number. The central region of the spectrum is enlarged in the inset at the bottom on the right

Table 1 GFT and G^{2}FT NMR experiments recorded for subunit c (D61 → N) of the *E. coli* F_1F_0 ATP synthase

Experiment	Spectral parameters Indirect dimension:[a] t_{max} (ms); complex points; Digital Resolution (Hz/Point)[a]	Measurement time (hours)[b]	Peak detection yield (%)	Average S/N
GFT				
L-(4,3)D HNN$\underline{C}^{\alpha\beta}\underline{C}^{\alpha}$	$\omega_1(^{13}C^{\alpha}, ^{13}C^{\alpha\beta})$: 6.5; 78; 76.9 $\omega_2(^{15}N)$: 18.6; 26; 26.9	11.0 (130)	96	5.3 ± 6.2
L-(4,3)D HNN(CO)$\underline{C}^{\alpha\beta}\underline{C}^{\alpha}$	$\omega_1(^{13}C^{\alpha}, ^{13}C^{\alpha\beta})$: 6.5; 78; 76.9 $\omega_2(^{15}N)$: 18.6; 26; 26.9	10.5 (130)	98	5.4 ± 6.5
(3,2)D HN$\underline{NCO}$	$\omega_1(^{15}N, ^{13}C')$: 40 ; 64; 19.5	0.25 (9.7)	100	16.7 ± 10.4
(4,2)D $\underline{HACA}$(CO)$\underline{N}$HN	$\omega_1(^{15}N, ^{13}C', ^{13}C^{\alpha})$: 6.6; 53; 15.5	3.0 (258)	100	11.1 ± 8.5
(4,3)D $\underline{HCCH}$	$\omega_1(^{13}C, ^{1}H)$: 6.6; 100; 75 $\omega_2(^{13}C)$: 5.3; 24; 94	8.5 (137)	96	15.9 ± 16.8
NOESY				
3D ^{15}N, $^{13}C^{alip}$, $^{13}C^{aro}$-resolved [^{1}H,^{1}H]-NOESY	$\omega_1(^{1}H)$: 15.5; 140; 32 $\omega_2(^{13}C)$: 6.6; 36; 75 $\omega_2(^{15}N)$: 20.5; 36; 24.3	9.5	100	6.5 ± 6.7[c]
Total NOESY and GFT		~43		
G^{2}FT				
(5,3)D HN{$\underline{N,CO}$}{$\underline{C}^{\alpha\beta}\underline{C}^{\alpha}$}	$\omega_1(^{13}C^{\alpha}, ^{13}C^{\alpha\beta})$: 6.5; 78; 76.9 $\omega_2(^{15}N, ^{13}C')$: 18.7; 30; 26.7	55 (7,750)	100	3.1 ± 3.3
(5,3)D {$\underline{C}^{\alpha\beta}\underline{C}^{\alpha}$}{$\underline{CON}$}HN	$\omega_1(^{13}C^{\alpha}, ^{13}C^{\alpha\beta})$: 6.5; 78; 76.9 $\omega_2(^{15}N, ^{13}C')$: 15.6; 25; 32	20 (5,380)	100	11.4 ± 11.4

[a] Direct dimension: $\omega_3(^{1}H)$: 64; 512; 8

[b] Minimal measurement time of the conventional congener having the same spectral resolution (i.e., the same t_{max} values for the indirect dimensions) are given in parentheses. Those were calculated using equivalent spectral widths, as well as the same number of transients, relaxation delay between scans and maximal evolution periods as the GFT NMR experiments

[c] Diagonal and intra-residue cross peaks were excluded

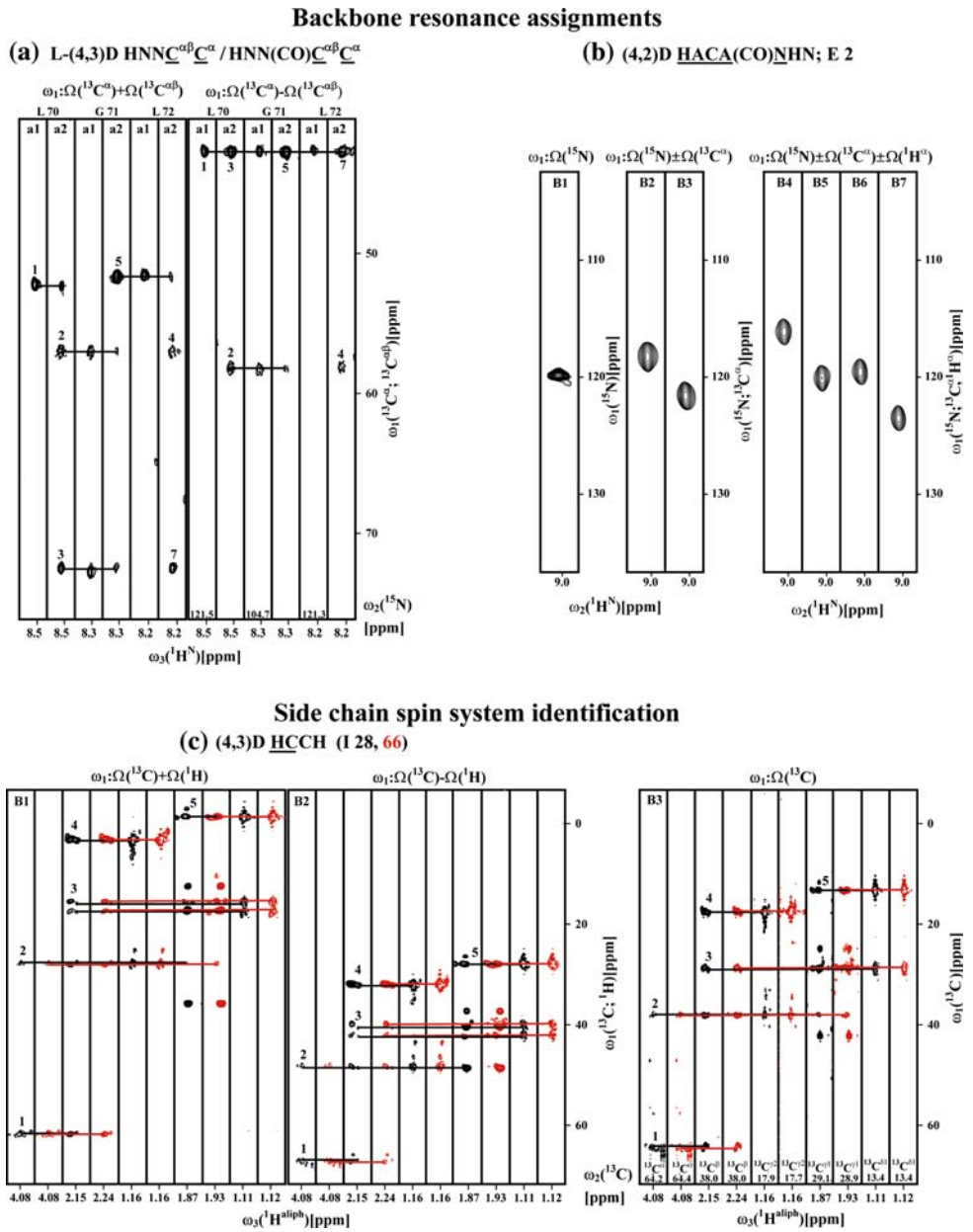

15–20 kDa (Krueger-Koplin et al. 2004). Consistently, we obtained for the present study at 45°C an approximate isotropic overall rotational correlation time, τ_r, of ~11 ns as inferred from ^{15}N nuclear spin relaxation time $T_1/T_{1\rho}$ ratios (e.g. Szyperski et al. 2002).

All NMR experiments were recorded at a temperature of 45°C on a Varian INOVA 600 spectrometer equipped with a cryogenic ^{1}H{^{13}C, ^{15}N} triple resonance probe (Table 1): (3,2)D HNNCO, longitudinal relaxation optimized L-(4,3)D HNN$C^{\alpha\beta}C^{\alpha}$ and L-(4,3)D HNN(CO)$C^{\alpha\beta}C^{\alpha}$ (Atreya and Szyperski 2004), (4,2)D HACA(CO)NHN (Kim and Szyperski 2003), and (4,3)D HCCH (Liu et al. 2005) were acquired along with simultaneous 3D ^{15}N, $^{13}C^{aliphatic}$, $^{13}C^{aromatic}$-resolved [^{1}H,^{1}H]-NOESY (Xia et al. 2003; Shen et al. 2005). This protocol enables one to adapt measurement times to sensitivity requirements while obtaining high-dimensional spectral information and keeping the number of experiments small: the total measurement time was only ~43 h. In spite of the short measurement times, nearly complete peak detection and sufficiently large S/N ratios were registered (Table 1).

The program PROSA (Güntert et al. 1992) was used for data processing and the program XEASY (Bartels et al. 1995) was used for spectral analysis. For backbone HN-N-CO spin system identification, 2D [^{15}N,^{1}H] HSQC (Fig. 2) and (3,2)D HNNCO were used. Sequential backbone and $^{13}C^{\beta}$ resonance assignments were performed as was described for soluble globular proteins (Liu et al. 2005)

◀ **Fig. 3** Resonance assignment of subunit c based on GFT experiments (Table 1). (**a**) [$\omega_1(^{13}C^{\alpha}$, $^{13}C^{\alpha\beta}$),$\omega_3(^1H^N)$]-strips taken from L-(4,3)D HNN(CO)C$^{\alpha\beta}$C$^{\alpha}$NH (labeled with a1) and L-(4,3)D HNNC$^{\alpha\beta}$C$^{\alpha}$ (labeled with a2) at $\omega_2(^{15}N)$ (the ^{15}N chemical shifts are indicated at the bottom of the strips) of residues 70–72 (referred to as residue *i*). The strips are centered along $\omega_3(^1H^N)$ about their backbone $^1H^N$ shifts. Along $\omega_1(^{13}C^{\alpha}$, $^{13}C^{\alpha\beta})$, peaks are observed at $\Omega(^{13}C^{\alpha}) \pm \Omega(^{13}C^{\alpha/\beta})$ of residue $i-1$ in "a1" and of residue i in "a2" (in addition, peaks originating from residue $i-1$ are observed in "a2" if transfer via $^2J_{NC\alpha}$ is sufficiently effective). $\Omega(X)$ (X = $^{13}C^{\alpha}$, $^{13}C^{\beta}$) denotes the offset relative to the carrier position [during $t_1(^{13}C^{\alpha\beta})$, the ^{13}C carrier frequency is placed at 43 ppm; during $t_1(^{13}C^{\alpha})$, the carrier frequency is placed at 56 ppm]. The composite plot of strips *on the left* was taken from the GFT sub-spectrum comprising peaks at $\Omega(^{13}C^{\alpha}) + \Omega(^{13}C^{\alpha})$ (labeled as 1, 3, 5, 7) and $\Omega(^{13}C^{\alpha}) + \Omega(^{13}C^{\beta})$ (labeled as 2, 4), and the composite plot *on the right* was taken from the sub-spectrum comprising peaks at $\Omega(^{13}C^{\alpha}) - \Omega(^{13}C^{\alpha})$ (1, 3, 5, 7) and $\Omega(^{13}C^{\alpha}) - \Omega(^{13}C^{\beta})$ (2, 4) (the type of linear combination of chemical shifts is indicated above the composite plots). The combined use of L-(4,3)D C$^{\alpha\beta}$C$^{\alpha}$(CO)NH/HNNC$^{\alpha\beta}$C$^{\alpha}$ yields three sequential walks along the polypeptide backbone which are indicated by dashed lines. Peaks were sequentially assigned to the $^{13}C^{\prime}$shifts of G69 (1), L70 (2, 3), G71 (5), and L72 (4, 7). (**b**) Composite plots of strips taken from (4,2)D HACA(CO)NHN used for $^1H^{\alpha}$ resonance assignment. The signals in panel (b) arise from magnetization transfer from $^1H^{\alpha}$ of M1 to $^1H^N$ of E2. The four basic spectra (labeled B4-B7) encode the chemical shifts of $^1H^{\alpha}_{i-1}$, $^{13}C^{\alpha}_{i-1}$, and $^{15}N_i$ in a single GFT dimension: linear combinations are registered as $\Omega_0 \pm \Omega_1 \pm \Omega_2$ with $\Omega_0 = \Omega(^{15}N)$, $\Omega_1 = \Omega(^{13}C^{\alpha})$ and $\Omega_2 = \Omega(^1H^{\alpha})$ (the part per million scale along ω_1 is defined for ^{15}N). Specifically, the linear combinations observed in sub-spectra B4–B7 are: B4 $[\Omega_0 + \Omega_1 + \Omega_2]$; B5 $[\Omega_0 + \Omega_1 - \Omega_2]$; B6 $[\Omega_0 - \Omega_1 + \Omega_2]$; B7 $[\Omega_0 - \Omega_1 - \Omega_2]$. To resolve potential shift degeneracies, first-order central peak spectra are acquired (B2–B3) comprising peaks at: B2 $[\Omega_0 + \Omega_1]$; B3 $[\Omega_0 - \Omega_1]$, second-order central peaks (B1) are signals of 2D [^{15}N, ^1H]-HSQC at Ω_0. (**c**) Assignment of aliphatic side chains exemplified for I28 (black) and I66 (red): the chemical shifts are nearly degenerate and only the 4D spectral information enables efficient resonance assignment. On the left, two composite plots show strips taken from the basic sub-spectra providing $\Omega(^{13}C) + \Omega(^1H)$ (labeled B1) and $\Omega(^{13}C) - \Omega(^1H)$ (B2) along the GFT dimension ω_1 (Table 1). On the right, a composite plot (B3) shows strips taken from the central peak spectrum of (4,3)D HCCH, providing $\Omega(^{13}C)$ along ω_1 [that is, 3D (H)CCH information]. For aliphatic spin system identification, sums and differences of shifts of covalently attached ^{13}C and ^1H nuclei are delineated in B1 and B2, while ^{13}C shifts are matched in B3. The five $[\omega_1(^{13}C, ^1H),\omega_3(^1H)]$ strips were taken along $\omega_2(^{13}C)$ at the shifts of $^{13}C^{\alpha}$, $^{13}C^{\beta}$, $^{13}C^{\gamma 1}$, $^{13}C^{\gamma 2}$, and $^{13}C^{\delta 1}$ (indicated at the bottom of the strips of B3). The peaks encode along ω_1 linear combinations of the following shifts: $^{13}C^{\alpha}/^1H^{\alpha}$(labeled as 1), $^{13}C^{\beta}/^1H^{\beta}$(2), $^{13}C^{\gamma 12,\gamma 13}/^1H^{\gamma 12,\gamma 13}$ (3), $^{13}C^{\gamma 2}/^1H^{\gamma 2}$ (4), and $^{13}C^{\delta}/^1H^{\delta}$ (5)

based on L-(4,3)D HNNC$^{\alpha\beta}$C$^{\alpha}$, L-(4,3)D HNN(CO)C$^{\alpha\beta}$C$^{\alpha}$ and (4,2)D HACA(CO)NHN. Side-chain resonance assignment relied on (4,3)D HCCH (Liu et al. 2005) and simultaneous 3D ^{15}N, $^{13}C^{aliphatic}$, $^{13}C^{aromatic}$-resolved [^1H,^1H]-NOESY. Data analysis resulted in sequence specific assignments (BMRB accession number: 15564) (Fig. 3a) for (i) all backbone and $^{13}C^{\beta}$ shifts (excluding only those of the terminal NH_3^+ group, the ^{15}N shifts of proline residues, and the $^{13}C^{\prime}$ shifts of residues preceding proline residues), and (ii) 97% of the side chain resonance (Fig. 3c) (excluding only K NH_3^+, R NH_2, and OH groups). Secondary chemical shifts of $^{13}C^{\alpha}$ and $^{13}C^{\beta}$, that is their deviation from random coil values (e.g. Zhang et al. 2003), correlate with protein backbone conformation (Spera and Bax 1991): downfield and upfield shifts are observed, respectively, for $^{13}C^{\alpha}$ and $^{13}C^{\beta}$ in α-helices of globular proteins. On the average, the secondary shifts are 3.09 ± 1.00 ppm for $^{13}C^{\alpha}$ and -0.38 ± 0.85 ppm for $^{13}C^{\beta}$ (Spera and Bax 1991). For subunit c we obtained 2.59 ± 0.96 ppm and -0.65 ± 0.70 ppm, indicating that the secondary shifts in transmembrane helices are not significantly different from what is observed for globular proteins (see also Chill et al. 2006).

When using conventional 3D NMR (Cavanagh et al. 2007), nearly complete resonance assignment of α-helical membrane proteins requires long measurement times. This is because high degeneracy of the $^1H^{\alpha}/^{13}C^{\alpha}$ as well as side chain $^{13}C/^1H$ shifts requires acquisition of a larger number of different experiments. The resonance assignment of subunit c by use of conventional experiments relied on the following eight 3D experiments to accomplish comparable assignment completeness, where the number of increments in the indirect dimensions is indicated in parentheses: 3D HNNCO (^{15}N: 22 complex points, $^{13}C^{\prime}$: 50), HNNCACB (^{15}N: 22, $^{13}C^{\alpha/\beta}$: 60), HNN(CO)CACB (^{15}N: 22, $^{13}C^{\alpha/\beta}$: 60), H(C)CH (^1H: 100, ^{13}C: 64), H(C)CH-TOCSY (^1H: 90, ^{13}C: 87), 3D ^{15}N-resolved [^1H,^1H]-NOESY (^1H: 170, ^{15}N: 32), 3D $^{13}C^{aliphatic}$-resolved [^1H,^1H]-NOESY (^1H: 150, ^{13}C: 40) and 3D $^{13}C^{aromatic}$-resolved [^1H,^1H]-NOESY (^1H: 128, ^{13}C: 29). Thus, data acquisition (with 4 or 8 transients per increment in 368 h using a conventional probe) required recording of a total of 132,488 averaged transients. In comparison, only 72,488 averaged transients where acquired for the NMR data of Table 1, showing that GFT NMR and simultaneous NOESY data acquisition reduced the minimal measurement about twofold. At the same time, highly resolved 4D spectral information was encoded in the GFT NMR experiments (see Table 1 for a comparison with the minimal measurement times of the conventional congener experiments). This also greatly enhances the speed and reliability of the resonance assignment process, again by breaking the high shift degeneracy typically encountered for α-helical membrane proteins. For example, the chemical shifts of subunit c could be assigned within a week, whereas the analysis time for the larger set of conventional data was several weeks.

To assess their efficiency for resonance assignment of membrane proteins, two G^{2}FT NMR experiments (Atreya et al. 2005), i.e., (5,3)D HN{N,CO}{C$^{\alpha\beta}$C$^{\alpha}$} and (5,3)D {C$^{\alpha\beta}$C$^{\alpha}$}{CON}HN for breaking the very high chemical shift degeneracy encountered for such systems were also recorded. The lower intrinsic sensitivity of these experiments, each of which delivers 5D spectral information, required somewhat longer measurement times in order to

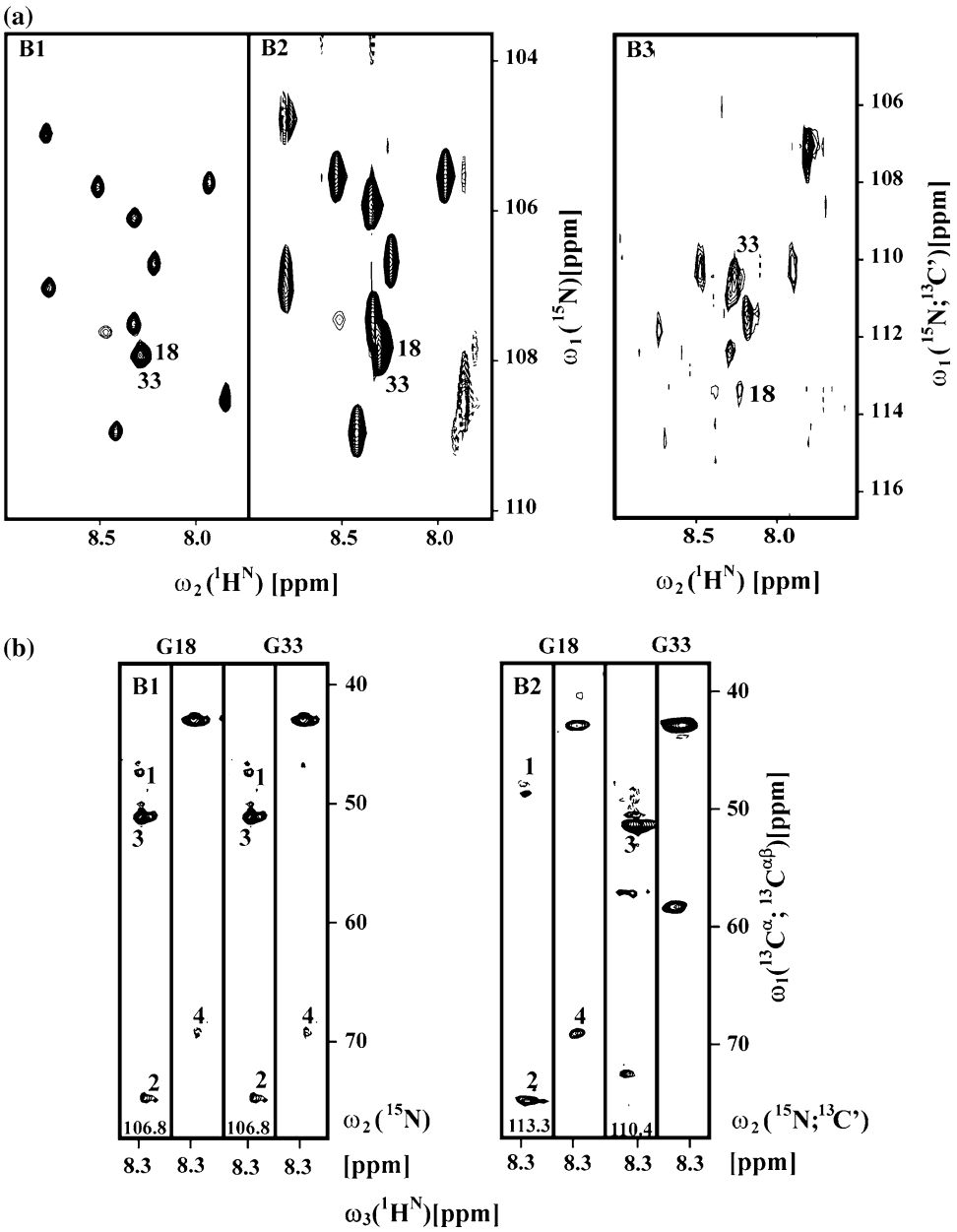

Fig. 4 (**a**) Plots of spectral regions comprising signals arising from G18 and G33 taken from (B1) 2D [^{15}N, ^{1}H]-HSQC, (B2) projection of L-(4,3)D HNN(CO)C$^{\alpha\beta}$C$^{\alpha}$ along the GFT-dimension, (B3) projection of (5,3)D {C$^{\alpha\beta}$C$^{\alpha}$}{CON}HN along the {C$^{\alpha\beta}$C$^{\alpha}$}-GFT-dimension. In (B1) and (B2) signals from G18 and G33 are overlapped, while they are resolved at $\Omega(^{15}\mathrm{N}) + \Omega\,(^{13}\mathrm{C}')/4$ in (B3) due to non-degenerate $^{13}\mathrm{C}'_{i-1}$ shifts. (**b**) [$\omega(^{13}\mathrm{C}^{\alpha}$, $^{13}\mathrm{C}^{\alpha\beta}$), $\omega_3(^{1}\mathrm{H}^{\mathrm{N}})$] strips taken from GFT L-(4,3)D HNN(CO)C$^{\alpha\beta}$C$^{\alpha}$ (B1) and G^{2}FT (5,3)D {C$^{\overline{\alpha\beta}}C^{\overline{\alpha}}$}{CON}HN (B2) were taken, respectively, at $\omega_2(^{15}\mathrm{N})$ and $\omega_2(^{15}\mathrm{N};\,^{13}\mathrm{C}')$ of residues G18 (peaks '1', '2', '4') and G33 (peaks '3'). The peaks are observed at $\Omega(^{13}\mathrm{C}^{\alpha}) \pm (^{13}\mathrm{C}^{\alpha/\beta})$ of residue $i-1$. The peaks in (B1) arise from G18 and G33 having degenerate ^{15}N and ^{1}H shifts; peaks are resolved in (B2) due to non-degenerate $^{13}\mathrm{C}'_{i-1}$ shifts

ensure (nearly) complete peak detection and workable S/N ratios (Table 1). Importantly, however, the G^{2}FT NMR experiments are $^{13}\mathrm{C}'_{i-1}$, $^{15}\mathrm{N}_i$,$^{1}\mathrm{H}^{\mathrm{N}}{}_i$-resolved, that is, $^{15}\mathrm{N}_i$ and $^{13}\mathrm{C}'_{i-1}$ shifts are jointly sampled for breaking ^{15}N,$^{1}\mathrm{H}^{\mathrm{N}}$-shift degeneracy, while $^{13}\mathrm{C}^{\alpha/\beta}$ and $^{13}\mathrm{C}^{\alpha}$ shifts are jointly sampled for sequentially linking spin systems (Fig. 4). Evidently, the (5,3)D G^{2}FT experiments can be combined with ^{15}N-resolved (4,3)D counterparts (Fig. 3b). Hence, in the sub-spectra constituting (5,3)D HN{N,CO}{C$^{\alpha\beta}$C$^{\alpha}$}, (5,3)D {C$^{\alpha\beta}$C$^{\alpha}$}{CON}HN, L-(4,3)D HNNC$^{\alpha\beta}$C$^{\alpha}$ and L-(4,3)D HNN(CO)C$^{\alpha\beta}$C$^{\alpha}$ nine 'sequential walks' can be established.

Taken together, protocols based on (L-optimized) GFT and G^{2}FT NMR promise to be highly valuable for assigning larger, possibly deuterated α-helical membrane proteins, particularly in high throughput structural genomics efforts.

Acknowledgements This work was supported by the National Institutes of Health (U54 GM074958-01) and the National Science Foundation (MCB 0416899). We thank Mr. Yu-Chieh Lin for help with the NMR sample preparation.

References

Atreya HS, Szyperski T (2004) G-matrix Fourier transform NMR spectroscopy for complete protein resonance assignment. Proc Natl Acad Sci USA 101:9642–9647

Atreya HS, Szyperski T (2005) Rapid NMR data collection. Methods Enzymol 394:78–108

Atreya HS, Eletsky A, Szyperski T (2005) Resonance assignment of proteins with high shift degeneracy based on 5D spectral information encoded in G^2FT NMR experiments. J Am Chem Soc 127:4554–4555

Bartels C, Xia T, Billeter M, Guntert P, Wüthrich K (1995) The program XEASY for computer-supported NMR spectral analysis of biological macromolecules. J Biomol NMR 6:1–10

Cavanagh J, Fairbrother WJ, Palmer AG III, Rance M, Skelton NJ (2007) Protein NMR Spectroscopy. Elsevier Academic Press, San Diego, CA

Chill JH, Louis JM, Miller C, Bax A (2006) NMR study of the tetrameric KcsA potassium channel in detergent micelles. Protein Sci 15:684–698

Dmitriev OY, Fillingame RH (2001) Structure of Ala(20) → Pro/Pro(64) → Ala substituted subunit c of *Escherichia coli* ATP synthase in which the essential proline is switched between transmembrane helices. J Biol Chem 276:27449–27454

Dmitriev OY, Abildgaard F, Markley JL, Fillingame RH (2002) Structure of Ala24/Asp61 → Asp24/Asn61 substituted subunit c of *Escherichia coli* ATP synthase: implications for the mechanism of proton transport and rotary movement in the F_0 complex. Biochemistry 41:5537–5547

Eghbalnia HR, Bahrami A, Tonelli M, Hallenga K, Markley JL (2005) High-resolution iterative frequency identification for NMR as a general strategy for multidimensional data collection. J Am Chem Soc 127:12528–12536

Eletsky A, Atreya HS, Liu G, Szyperski T (2005) Probing structure and functional dynamics of (large) proteins with aromatic rings: L-GFT-TROSY (4,3)D HCCH NMR spectroscopy. J Am Chem Soc 127:14578–14579

Fernandez C, Hilty C, Wider G, Güntert P, Wüthrich K (2004) NMR structure of the integral membrane protein OmpX. J Mol Biol 336:1211–1221

Gao FP, Cross TA (2005) Recent developments in membrane protein structural genomics. Genome Biol 6:244

Girvin ME, Rastogi VK, Abildgaard F, Markley JL, Fillingame RH (1998) Solution structure of the transmembrane H^+-transporting subunit c of the F_1F_0 ATP synthase. Biochemistry 37:8817–8824

Granseth E, Seppälä S, Rapp M, Daley DO, Von Heijne G (2007) Membrane protein structural biology—how far can the bugs take us? Mol Membr Biol 24:329–332

Güntert P, Dötsch V, Wider G, Wüthrich K (1992) Processing of multi-dimensional NMR data with the new software PROSA. J Biomol NMR 2:619–629

Hiller S, Fiorito F, Wüthrich K, Wider G (2005) Automated projection spectroscopy (APSY). Proc Natl Acad Sci USA 102:10876–10881

Kim S, Szyperski T (2003) GFT NMR, a new approach to rapidly obtain precise high-dimensional NMR spectral information. J Am Chem Soc 125:1385–1393

Krueger-Koplin RD, Sorgen PL, Krueger-Koplin ST, Rivera-Torres AO, Cahill SM, Hicks DB, Grinius L, Krulwich TA, Girvin ME (2004) An evaluation of detergents for NMR structural studies of membrane proteins. J Biomol NMR 28:43–57

Kupce E, Freeman R (2004) Projection-reconstruction technique for speeding up multidimensional NMR spectroscopy. J Am Chem Soc 126:6429–6440

Liu GH, Shen Y, Atreya HS, Parish D, Shao Y, Sukumaran DK, Xiao R, Yee A, Lemak A, Bhattacharya A, Acton T, Arrowsmith C, Montelione G, Szyperski T (2005) NMR data collection and analysis protocol for high-throughput protein structure determination. Proc Natl Acad Sci USA 102:10487–10492

Lundstrom K (2007) Structural genomics and drug discovery. J Cell Mol Med 11: 224–238

Matthey U, Kaim G, Braun D, Wüthrich K, Dimroth P (1999) NMR studies of subunit c of the ATP synthase from *Propionigenium modestum* in dodecylsulphate micelles. Eur J Biochem 261: 459–467

Matthey U, Braun D, Dimroth P (2002) NMR investigations of subunit c of the ATP synthase from *Propionigenium modestum* in chloroform/methanol/water (4:4:1). Eur J Biochem 269: 1942–1946

Nakano T, Ikegami T, Suzuki T, Yoshida M, Akutsu H (2006) A new solution structure of ATP synthase subunit c from thermophilic *Bacillus* PS3, suggesting a local conformational change for H^+-translocation. J Mol Biol 358:132–144

Norwood TJ, Crawford DA, Steventon ME, Driscoll PC, Campbell ID (1992) Heteronuclear ^1H-^{15}N nuclear magnetic resonance studies of the c subunit of the *Escherichia coli* F_1F_0 ATP synthase: assignment and secondary structure. Biochemistry 31: 6285–6290

Rastogi VK, Girvin ME (1999a) ^1H, ^{13}C, and ^{15}N assignments and secondary structure of the high pH form of subunit c of the F_1F_0 ATP synthase. J Biomol NMR 13:91–92

Rastogi VK, Girvin ME (1999b) Structural changes linked to proton translocation by subunit c of the ATP synthase. Nature 402: 263–268

Rivera-Torres IO, Krueger-Koplin RD, Hicks DB, Cahill SM, Krulwich TA, Girvin ME (2004) pKa of the essential Glu54 and backbone conformation for subunit c from the H^+-coupled F_1F_0 ATP synthase from an alkaliphilic *Bacillus*. FEBS Lett 575:131–135

Shannon CE (1948) A mathematical theory of communication. Bell Syst Tech J 27:379–423

Shen Y, Atreya HS, Liu G, Szyperski T (2005) G-matrix Fourier transform NOESY based protocol for high-quality protein structure determination. J Am Chem Soc 127:9085–9099

Sorgen PL, Hu Y, Guan L, Kaback HR, Girvin ME (2002) An approach to membrane protein structure without crystals. Proc Natl Acad Sci USA 99:14037–14040

Spera S, Bax A (1991) Empirical correlation between protein backbone conformation and C-Alpha and C-Beta C-13 nuclear-magnetic-resonance chemical shifts. J Am Chem Soc 113: 5490–5492

Szyperski T, Atreya HS (2006) Principles and applications of GFT projection NMR spectroscopy. Magn Reson Chem 44:S51–S60

Szyperski T, Yeh DC, Sukumaran DK, Moseley HNB, Montelione GT (2002) Reduced-dimensionality NMR spectroscopy for high-throughput protein resonance assignment. Proc Natl Acad Sci USA 99:8009–8014

Tamm LK, Abildgaard F, Arora A, Blad H, Bushweller JH (2003) Structure, dynamics and function of the outer membrane protein A (OmpA) and influenza hemagglutinin fusion domain in detergent micelles by solution NMR. FEBS Lett 555:139–143

Tourasse NJ, Li WH (2000) Selective constraints, amino acid composition, and the rate of protein evolution. Mol Biol Evol 17:656–664

Xia YL, Yee A, Arrowsmith CH, Gao XL (2003) H-1(C) and H-1(N) total NOE correlations in a single 3D NMR experiment. N-15 and C-13 time-sharing in t(1) and t(2) dimensions for simultaneous data acquisition. J Biomol NMR 27:193–203

Zhang HY, Neal S, Wishart DS (2003) RefDB: a database of uniformly referenced protein chemical shifts. J Biomol NMR 25:173–195